![TUDelft logo]

Delft University of Technology

Experimental and simulation-based investigations of marine diesel engine performance against static back pressure

Sapra, Harsh; Godjevac, Milinko; Visser, Klaas; Stapersma, Douwe; Dijkstra, Chris

Important note
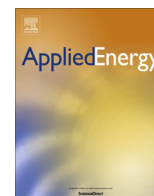To cite this publication, please use the final published version (if applicable).
Please check the document version above.

Experimental and simulation-based investigations of marine diesel engine performance against static back pressure

Harsh Sapra [a,*], Milinko Godjevac [a], Klaas Visser [a], Douwe Stapersma [a], Chris Dijkstra [b]

[a] Faculty of Mechanical, Maritime and Materials Engineering, Delft University of Technology, The Netherlands
[b] Netherlands Defence Academy, Den Helder, The Netherlands

HIGHLIGHTS

- Combination of experiments and MVEM to study effects of back pressure on marine engine performance.
- Method applying smoke limit and thermal overload to define ceiling of acceptable back pressures.
- Two different turbocharging technologies and valve overlaps to tackle 1 mWC of back pressure.

ARTICLE INFO

ABSTRACT

After-treatment technologies are adopted in automobiles and ships to meet strict emission regulations, which increase exhaust back pressure. Furthermore, underwater exhaust systems are employed on board ships to save space, and reduce noise and pollution on working decks. However, water at exhaust outlet creates a flow resistance for the exhaust gases, which adds to the back pressure. High back pressure reduces the operating limits of an engine, increases fuel consumption, and can lead to exhaust smoke. While the effects of back pressure were recognized earlier, there is a lack of experimentally validated research on the performance limits of a turbocharged, marine diesel engine against high back pressure for the entire operating window. The focus of this research is to provide a comprehensive understanding of back pressure effects on marine diesel engine performance, and to identify limits of acceptable back pressure along with methods to tackle high back pressure.

In this work, a pulse turbocharged, medium speed, diesel engine was tested at different loads and engine speeds; against different values of static back pressure. Additionally, mean value model simulations could be validated and were used to compare the performance of a pulse and constant pressure turbocharged engine against high back pressures of 1 meter water-column (mWC), and for two different values of valve overlap.

Using the validated simulation model, the conceptual basis for the engine smoke limit as well as for thermal overloading is investigated. A methodology applying the conceptual basis to define boundaries of acceptable back pressures has been presented in this paper. A combination of pulse turbocharger systems and small valve overlap showed to significantly improve back pressure handling capabilities of engines.

1. Introduction

Diesel engines are being widely applied in the power generation and transportation sector. Attributes such as operation simplicity, robust design and better fuel economy make diesel engines more appealing compared to most other prime movers. Since their invention in 1892, diesel engines have improved significantly in terms of power-to-space ratio, efficiency, fuel economy, reliability, etc. Performance of these engines enhanced with better understanding of physical and chemical processes taking place in an engine. Modelling of these engine processes has played a significant role in expanding our knowledge. With the advent of powerful computers, researchers use engine models to improve understanding of engine performance, combustion, closed in-cylinder process, gas exchange, etc. [1–3]. Furthermore, these models are also used to test different solutions (technologies) or control strategies that can help reduce fuel consumption, increase power output, reduce emissions to meet emission requirements [4–7]. In a similar fashion, this work presents a mean value engine model to study the

* Corresponding author.
  E-mail address: h.d.sapra@tudelft.nl (H. Sapra).

Nomenclature

p	pressure (bar)
$\bar{p}$	mean pressure
T	temperature (K)
M	torque (Nm)
α	mass-flow or area correction factor
β	power correction factor
ṁ	mass-flow rate (kg/s)
W	work (J)
C_{pulse}	pulse correction factor
Π	pressure ratio
τ	temperature ratio
η	speed (rpm)
χ	ratio of specific heats of air and exhaust gas
afr	air-to-fuel ratio
δ	fuel addition factor
λ	air-excess ratio

Subscripts

com	compressor
tur	turbine
ac	air-cover
cac	charger-air cooler
cyl	cylinder
eng	engine
Turbo/TC	turbocharger
OR	outlet-receiver
IR	inlet receiver
exh	exhaust
sv	silencer volume
amb	ambient
const	constant pressure turbocharger system

pulse	pulse pressure turbocharger system
d	discharge
e	exhaust/turbine outlet pressure
max	maximum
min	minimum
m	measurement
s	simulations
s	scavenge factor (in ection 5)
a	air
fresh	total incoming fresh air in the cylinder
a,min	minimum air required for complete combustion
eV	exhaust valve
est	estimator

Acronyms

MVEM	mean value engine model
mWC	meter of water-column
IMO	international maritime organization
SCR	selective catalytic reactors
BP	back pressure (mWC)
EXT	external

Units

mbar	millibar
kW	kilowatt
rpm	revolutions per minute
K	kelvin
kg/s	kilogram per second
s	second
m	meter

effects of back pressure on engine performance and test different solutions to tackle increased back pressure caused by exhaust gas after-treatment technologies, for instance.

Currently, in automobiles and ships, exhaust systems are equipped with end-of-pipe-technologies to reduce harmful emissions. For instance, ship emissions have been subjected to strict restrictions by IMO TIER III regulations, which are applicable from 1 January 2016 [8]. According to engine manufacturers, TIER III emission regulations can be met by retrofitting marine engines with exhaust gas after-treatment technologies such as scrubbers and/or selective catalytic reactors (SCR) [9,10]. However, after-treatment technologies cause a pressure loss in the exhaust piping [11]. Another trend in the maritime industry is to employ underwater exhaust systems, as they provide zero direct emissions to the atmosphere (emissions still exist), space saving, and reduction in noise and pollution on working decks. Other advantages of expelling underwater are decreased risk of hotspot detection for naval ships, and improved aesthetics of luxury ships due to elimination of bulky and un-appealing vertical exhaust funnels that pass through decks. However, exiting gases experience a flow resistance due to the pressure applied by the water at the outlet of underwater exhaust systems. The cumulative value of pressure loss or flow resistance in the exhaust system measured at the turbine outlet of a turbocharged engine or at the outlet of the exhaust manifold of a naturally aspirated engine is the back pressure felt by the engine.

For a given mechanical loading, back pressure is known to increase engine thermal loading and also fuel consumption. In extreme cases, the engine can also start smoking due to incomplete combustion, caused by lack of sufficient combustion-air inside the cylinder. Although back pressure effects on engine performance have been recognised before, few studies address the conse-

quences of marine engines running against high back pressure, especially due to underwater exhausts systems. For instance, Tauzia et al. provided a generic understanding of effects of dynamic back pressure due to partially submerged exhaust on marine diesel engine performance using model simulations [12]. Although the authors covered the effects of back pressure ranging from 0 to 6 metres of water column (600 mbar), a validated, quantitative analysis of back pressure on a real engine is not provided. Heild simulated the effects of back pressure on a turbocharged diesel engine used for submarine propulsion [13]. He showed that the effects of fluctuating back pressure are strongly non-linear and depend on the amplitude and period of the fluctuations. This study used the Ricardo Wave engine modelling software [14], and suggested the need of an experimental program to validate the results of the study before they can be relied upon. In a similar study, Ed Swain investigated variable area-nozzle turbocharging for a diesel engine in a diesel-electric submarine [15]. Michos et al. studied the performance of advanced turbocharging techniques against back pressure caused by fitting an Organic Rankine Cycle (ORC) in the exhaust line of a marine diesel engine [16]. The authors studied the performance only at full-load and rated engine speed.

All the above mentioned studies analysed engine performance using simulation models, and a few researches performed experiments to study engine performance against back pressure. For example, Joardder et al. [17] and Cong et al. [18] experimented on a naturally aspirated diesel engine running against back pressure. However, the effects on a turbocharged diesel engine will be different due to the difference in air-to-fuel ratios, delivered charge pressure, exhaust gas (exhaust receiver) temperatures, etc. Furthermore, Mittal et al. [19] tested the performance of a turbocharged diesel engine at constant engine speed, keeping the val-

ues of back pressure at lower loads, below 0.25 mWC. However, at lower power percentages (or rpms), a marine engine could be exposed to values of back pressure higher than 0.25 mWC, when running with underwater exhaust systems [20]. In [21], Burnete et al. studied the effects of back pressure on engine power, torque and exhaust gas opacity of a turbocharged diesel engine for generator applications. Besides these studies, some patents discussed the implementation of marine underwater exhaust [22–24]. Two studies describing the effects of exhaust system design on the performance of a naturally aspirated SI engine for automotive applications were also found [25,26].

The above literature study highlights a lack of experimentally validated research on marine diesel engine performance and its limits against back pressure. The literature study also revealed that a complete analysis Furthermore, a lack of methodology to define acceptable limits of back pressure that can be applied in practice was identified. Therefore, the goal of this paper is to provide an in-depth understanding of back pressure effects on marine diesel engine performance at different engine loads and speeds with the help of engine experiments and engine model simulations. The novelty of this paper is the methodology to apply a conceptual model of smoke and thermal overload to define a ceiling for acceptable back pressures that can be adopted in practice for any engine. Besides this, the paper also investigates capabilities of different turbocharger configurations along with different engine valve overlap settings to tackle high back pressures.
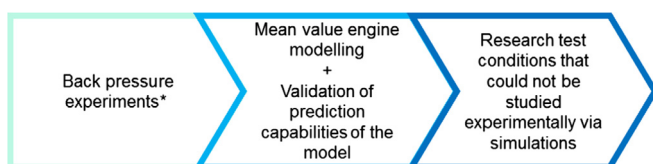
In this paper, the research methodology is described in Section 2, followed by the description of the test setup and the MVEM with a pulse turbocharger model. Section 3 covers model calibration and matching by simulating the performance of the pulse turbocharged test engine against no external back pressure. The effects of back pressure on engine performance based on measurements and model simulations are presented in Section 4. The paper concludes with a methodology to use smoke limit and thermal overloading to find allowable back pressure boundaries for the engine at different engine speeds. In addition to this, performance capabilities of pulse and constant pressure turbocharged engines against high back pressure are covered in Section 5.

2. Methodology, test setup and model description

The study of effects of back pressure on engine performance was carried out via experiments and simulations. The research methodology applied and the experimental test setup is described in this section, followed by a description of the MVEM used for the simulation studies. The section concludes with highlights of pulse turbocharger modelling and its implementation into the mean value model.

2.1. Methodology

In this research, engine model simulations along with experiments on a pulse turbocharged, medium speed, and 4-stroke diesel engine are used as tools to study effects of back pressure on engine performance. Fig. 2.1 shows the basic approach followed for this research. A Mean Value Engine Model (MVEM) is adopted to simulate engine performance against externally applied high back pressure, which could not be studied experimentally.

For the purpose of experiments, engine parameters were first measured at 9 different set-points (of load and engine speed), against three cases of back pressure. Fig. 2.2 depicts the 9 set-points measured. In the first case, engine performance with no externally applied back pressure was measured. The second and the third cases were for 0.25 mWC and 0.5 mWC of externally applied back pressure, respectively. For each case of back pressure, and at each set-point, engine parameters such as temperature, pressure, air flow-rate and fuel consumption were measured. The engine was allowed to settle for 15 min between each set-point and each case of externally applied back pressure, to make sure that all the engine parameters were stabilized before measuring.

The second step was to use engine measurements against no external back pressure, to calibrate and match the MVEM to simulate the performance of the test engine. Once calibrated and matched, the model was used to simulate the engine performance against the remaining two cases of back pressure. The simulations were then compared against test engine measurements to validate the model.

Furthermore, engine measurements were restricted to the maximum set-point of 340 kW at 981 rpm, while the actual rated power of this engine was 360 kW at 1000 rpm. However, MVEM was used to predict engine performance against back pressure at 360 kW and 1000 rpm. Thus, for all the results shown in this paper, 100 percent load point corresponds to 340 kW while the 105.9 percent load point corresponds to 360 kW, and 100 percent rpm percentage point (especially for results in Section 5) corresponds to 1000 rpm of engine speed.

Combination of experiments and simulation not only helped validate the prediction capabilities of the MVEM against back pressure, but also to study related engine performance. The validated model was used to understand and apply the concepts of smoke limit and thermal overloading to define back pressure limits. Lastly, the effect of different engine valve overlaps on engine performance against high back pressure, and capabilities of a pulse turbocharged and a constant pressure turbocharged engine at handling back pressure of 1 mWC, which could not be studied experimentally, were also investigated via model simulations.
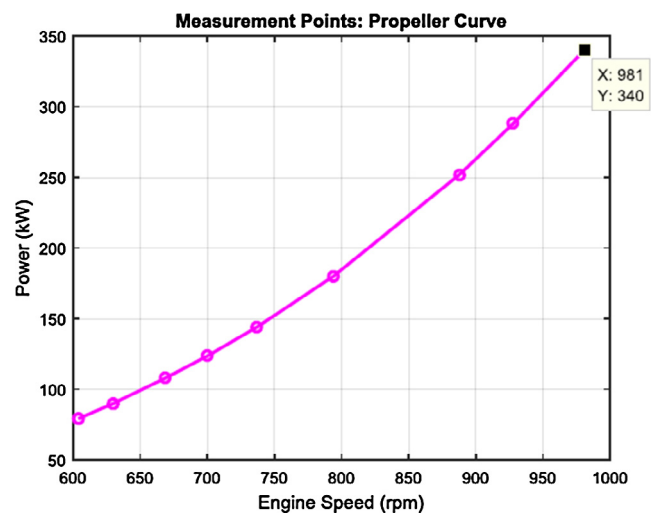

Fig. 2.1. Basic approach for this research.

Fig. 2.2. Measurement set-points along the propeller curve.

2.2. Test setup

Back pressure experiments are performed on a 4-stroke, pulse turbocharged and marine diesel engine. Table 2.1 lists the specifications of this test engine. The test engine is connected to a water-brake to apply the required load. In this manner, the engine is made to run at any set-point of speed and load. The engine governor keeps the engine at this specific engine speed point by controlling the fuel input in case of any back pressure fluctuations.

A manually operated butterfly valve, installed downstream of the turbine, is used to apply back pressure. Fig. 2.3 gives a schematic representation of the engine test setup, along with the locations at which different measurements of pressure, temperature and air flow are taken.

2.3. Mean value engine model (MVEM)

Researchers have adopted different schemes to model engine performance, which range from detailed computational fluid dynamic models to simple first order ones. The choice of modelling scheme depends on the amount of information required from the model, accuracy and computational time needed. Geertsma et al. [28] categorise different models based on the level of dynamics involved and underlying physical details. They classify them as

first order models, second order models, higher order mean value engine models [29–31] zero-dimensional crank angle models [32–34], one-dimensional fluid dynamics models [35] and multi-dimensional or computational fluid dynamics models [36–38]. Out of these, the crank angle models, one-dimensional fluid dynamics models and CFD models are complex and/or need high computational time, whereas the first and second order models miss out on vital information such as gas exchange and/or detailed turbocharger performance [39,40]. For the purpose of this research, the objective is to understand the effects of back pressure on overall engine parameters such as exhaust gas (exhaust receiver) temperatures, mass flow rates, manifold pressures, fuel consumption, etc. rather than the detailed in-cycle variations. Thus, the mean value engine model (MVEM) was chosen, which included the gas exchange model along with an analytical compressor-turbine model that proved vital when researching the effects of different engine valve overlaps and turbocharger configurations against back pressure.

The adopted model has been developed at Netherlands Defence Academy (NLDA) and Delft University of Technology (TU Delft). Different engine components such as the inlet volume, air-cover, inlet receiver, outlet receiver, cylinder and silencer/outlet volumes are modelled as a series of control volumes or 'volume elements'. These control volumes are connected to each other via resistances or 'resistance elements', as shown in Fig. 2.4. The control volumes calculate the instantaneous mass by integrating the net mass flow (conservation of mass), and the instantaneous temperature by integrating the net energy flow associated with the mass flows (conservation of energy). The instantaneous pressure of the element is calculated using the ideal gas law.

On the other hand, resistance elements estimate the mass flow as a function of pressure difference using the momentum equation. The cylinder volume is connected by one resistance element that models the sum of induction and scavenge mass flows through the engine. At the same time, empirical sub-models are used to calculate turbine and compressor characteristics. The primary output is engine torque; however, temperatures, pressures and mass flows can be obtained for different engine components. Furthermore, friction losses are calculated using an adaptation of the empirical formula given by Chen and Flynn [43], with adaptable coefficients, which are estimated to get the correct specific-fuel consumption. A

Table 2.1
Engine specifications [27].

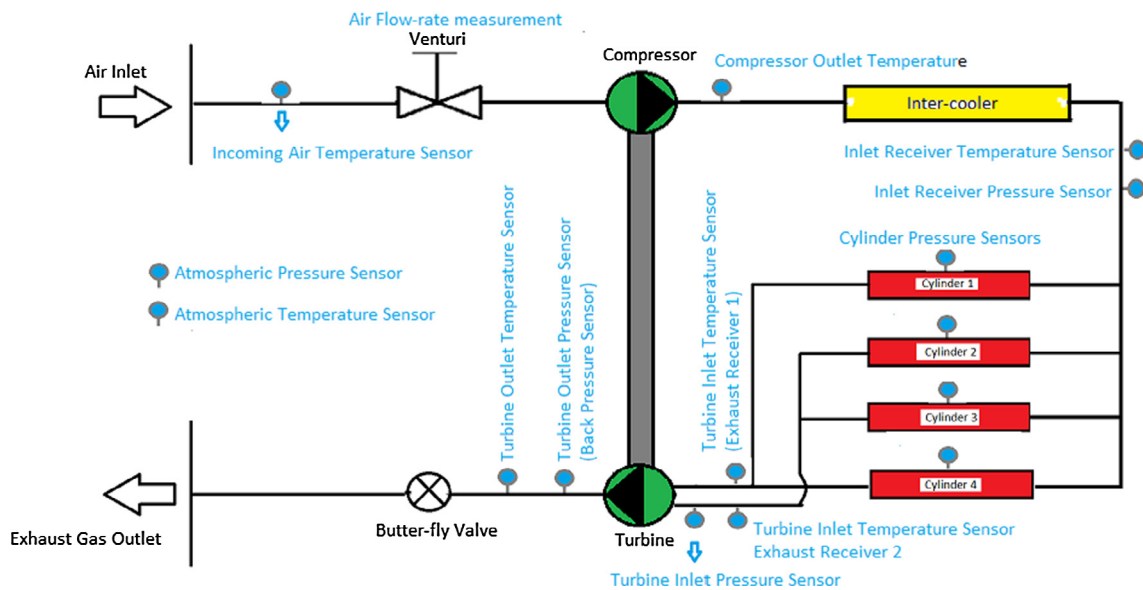| Parameters	
Engine model	MAN4L2027
Number of cylinders	4
Bore	0.20 m
Stroke	0.27 m
Rated speed	1000 rpm
Rated power	360 kW
Compression ratio	13.4
Fuel injection system	Plunger pump Direct injection
Turbocharger system	Pulse
Maximum back pressure	25 mbar (gauge)

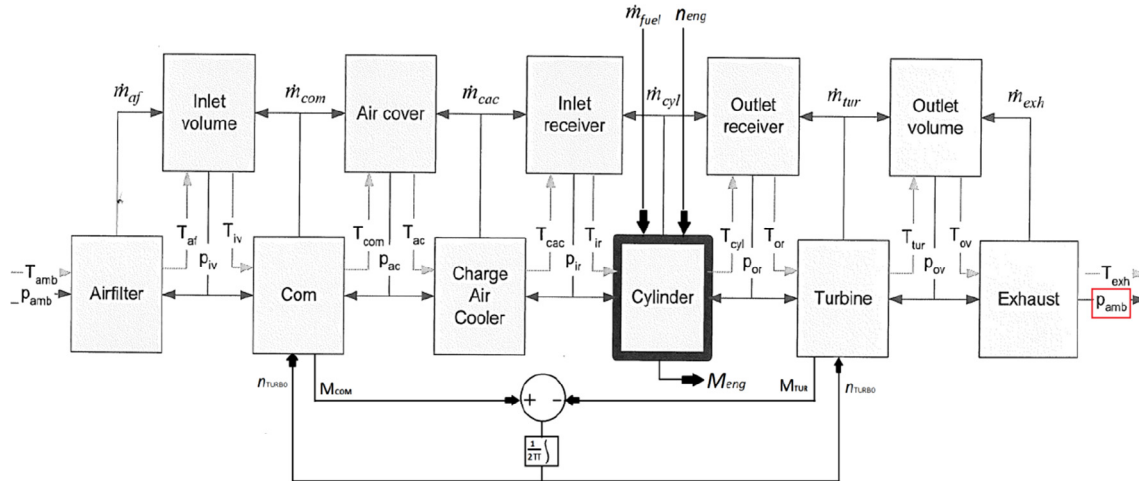**Fig. 2.3.** Outline of test setup and sensor placement.

Fig. 2.4. Mean value engine model [41,42].

detailed description of the model including the in-cylinder Seiliger model, gas exchange, model equations etc. can be found in [44–48]. The value of ambient pressure at exhaust outlet (p_{amb}), highlighted by a red box in Fig. 2.4, was converted into an input for the model to apply external back pressure ($p_{BP\_Applied}$). In this manner, the model was used to study engine performance against externally applied back pressure.

2.4. Extension of MVEM for pulse turbocharging

The test engine used for this research was equipped with a pulse turbocharger. Thus, a pulse turbocharger model was implemented in the MVEM. However, a pulse turbocharger system is not a mean value system. This is evident from Fig. 2.5, which shows a typical pressure pulse measured at the turbine inlet.

The MVEM used in this analysis has a pulse turbocharging model, which was originally developed by Baan [49]. The pulse model is based on the concept of pulse turbocharging given by Zinner [50], and is described in the following paragraphs.

In a pulse turbocharging system, the flow through the turbine reduces compared to that in case of a constant pressure system. Moreover, a pulse system turbine delivers more work than a con-
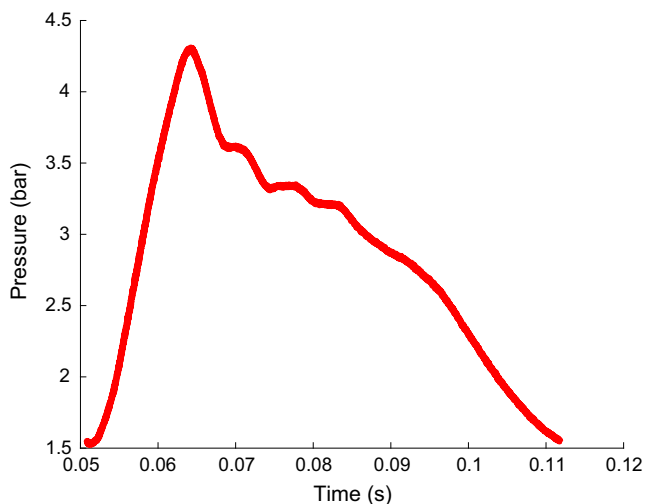
stant pressure system. This pulse effect of reduced mass flow and extra work is given by correction factors α and β, given by Eq. (1) and (2).

$$\alpha = \frac{\dot{m}_{tur,pulse}}{\dot{m}_{tur,const}} \tag{1}$$

$$\beta = \frac{\dot{W}_{tur,pulse}}{\dot{W}_{tur,const}} \tag{2}$$

where $\dot{W}_{tur,const}$ is the work rate for a constant pressure system and $\dot{m}_{tur,const}$ is the turbine mass-flow rate for a constant pressure system.

The values of α and β can be derived by analysing the turbine inlet pressure pulse. The simplest way of representing the pulse is by means of a block or a step function. The block pulse, shown in Fig. 2.6, is half the time at minimum discharge pressure and remaining at maximum discharge pressure.

In pulse turbocharging, the reduction in flow can be explained by the non-linear relation between flow and pressure difference. The maximum block pressure tends to reduce the flow, which is not compensated by a relatively larger flow during the low pressure block. Work rate, being flow times pressure difference, is non-linear and since the large pressure difference during the maximum block pressure dominates the flow in the product, work rate averaged over time increases due to the block pulse shape.

Zinner [50] showed with measurements that the correction factors α and β can be approximated as functions of a pulse factor,
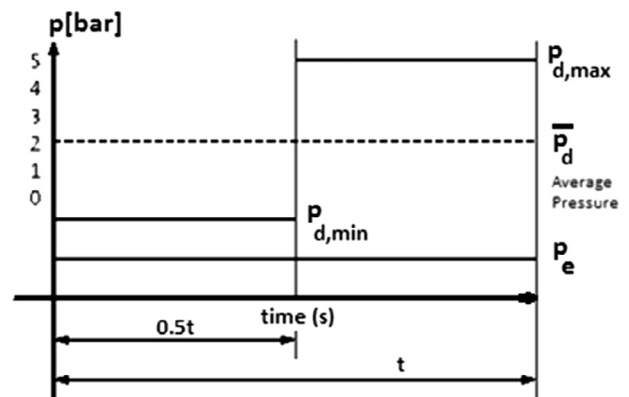

Fig. 2.5. Measured turbine inlet pressure pulse.
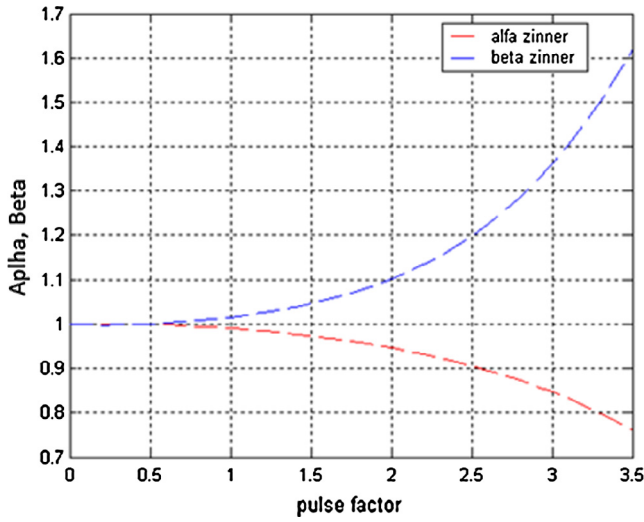

Fig. 2.6. Simplified (Step function) turbine inlet pressure pulse [51].

Fig. 2.7. Correction factors α and β as a function of the pulse factor suggested by Zinner, according to Stapersma [44,51].

Fig. 2.8. Discretization of measured turbine inlet pressure pulse at 340 kW and 981 rpm.

which is defined as the ratio of the difference between the maximum ($p_{d,max}$) and minimum pressure ($p_{d,min}$) of the pulse and the difference of the mean outlet receiver pressure ($\bar{p}_d$) and the turbine outlet pressure (p_e). The dependency of the correction factors on the pulse factor as suggested by Zinner is shown in Fig. 2.6, and mathematically represented by Eq. (3) and (4).

$$\alpha = f_1 \left(\frac{p_{d,max} - p_{d,min}}{\bar{p}_d - p_e} \right) \tag{3}$$

$$\beta = f_2 \left(\frac{p_{d,max} - p_{d,min}}{\bar{p}_d - p_e} \right) \tag{4}$$

Ligtvoet, following Zinner, realized that using a step-function to describe a pressure pulse is a very crude approximation [51]. Therefore, measured pulses were used to understand the effect of pulse in terms of α and β correction factors, in this research. The underlying equations for this analysis, which will be covered in the next paragraphs, can be found in [44,51].

For this analysis, the measured turbine inlet pressure pulse was discretized into multiple outlet receiver pressures, as shown in Fig. 2.8

For the pulse defined in Fig. 2.8, the correction factor α was calculated by comparing the mass flow through the turbine in case of constant receiver pressure (with mean constant pressure equal to mean of the pulse) to the sum of mass flows for different discharge pressures of the discrete pressure pulse.

$$\dot{m}_{tur,const} \sim \sqrt{\bar{p}_d - p_e} \tag{5}$$

$$\dot{m}_{tur,pulse} \sim \sum_{i=1}^{x} \sqrt{p_{d,i} - p_e} \tag{6}$$

where i = 1: number of discretized parts.

The dependency of mass flow rate ($\dot{m}_{tur}$) through the turbine on square root of pressure difference between outlet receiver pressure and turbine outlet pressure, is given by Stapersma in [14], and has been shown in Eq. (7).

$$\dot{m}_{tur} \sim \sqrt{\bar{p}_d - p_e} \tag{7}$$

Then, the correction factor (α) was calculated by using Eq. (8).

$$\alpha = \frac{\dot{m}_{tur,pulse}}{\dot{m}_{tur,const}} = \frac{\sum_{i=1}^{x} \sqrt{p_{d,i} - p_e}}{\sqrt{\bar{p}_d - p_e}} \tag{8}$$
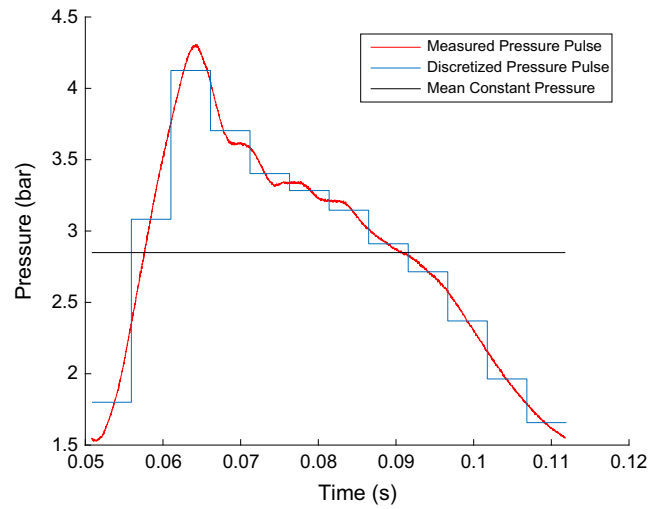
In a similar manner, β was calculated by applying Eq. (9).

$$\beta = \frac{\dot{W}_{tur,pulse}}{\dot{W}_{tur,const}} = \frac{\sum_{i=1}^{x} \dot{m}_{tur,pulse} \cdot (p_{d,i} - p_e)}{\dot{m}_{tur,const} \cdot (\bar{p}_d - p_e)} \tag{9}$$

Following this method, each turbine inlet pressure pulse, measured at the 9 set-points is discretised into 12 parts and used to calculate the values of α and β. The results are provided in Table 2.2.

Table 2.2 shows the values of α and β for the pulse system on the test bench engine. As expected, the values of α were found to be less than 1, while that of β were greater than 1. Thus, showing that for a pulse system the effective flow is lower and the effective turbine work is higher than that of a constant pressure system with the same mean pressure (as that of pulse) at the turbine inlet. In this way, the measured pressure pulses were used to derive the values of α and β correction factors given by Zinner. These values were then compared with simulated values of α and β, which were calculated in the model as a function of pulse factor using Fig. 2.7, and Eq. (3) and (4), given by Zinner.

However, in order to calculate the pulse factor from the parameters obtained from the MVEM, a modified pulse factor was adopted [52];

$$\text{Pulse factor}_{modified} = C_{pulse} \cdot \left(\frac{p_6 - p_{sv}}{\bar{p}_d - p_{sv}} \right) \tag{10}$$

Here, (the maximum pressure) p_6 is the pressure obtained from the Seiliger process, p_{sv} is the pressure at turbine outlet (silencer

Table 2.2
Values of α and β calculated from the discretization pulse.

RPM %	Load	Alpha	Beta
98.12	100	0.9763	1.06
92.83	84.7	0.9769	1.0629
88.79	74.11	0.9694	1.08455
79.37	52.94	0.9642	1.0867
73.68	42.35	0.9602	1.09529
70.0	36.32	0.9629	1.10425
66.9	31.76	0.9724	1.08267
62.99	26.47	0.9633	1.1046
60.37	23.23	0.9633	1.1527

volume), $\bar{p}_d$ is the mean pressure in the outlet receiver obtained from the MVEM. The calculated modified pulse factor is much higher than the pulse factor proposed by Zinner. Therefore, a pulse correction factor (C_{pulse}) is introduced. This C_{pulse} factor is used as a tuning factor to get the correct charge pressure while closely comparing the α and β values obtained from the measured pulse and simulations.

3. Calibration of the MVEM

In order to apply the MVEM to simulate conditions that could not be studied experimentally, the model first needs to be calibrated and matched to simulate the performance of the test engine. Therefore, this section briefly dicusses the setup of the MVEM and its calibration.

The MVEM is implemented in a MATLAB/Simulink environment and a number of parameters in principle must be specified. These parameters are arranged in an orderly set of parameter files and each file corresponds to a different component. For example, the 'cylinder_data.m' file contains all the parameters required to model the process within the cylinder. A pre-simulation creates a file 'initial_condition.mat' where the initial values of all engine model parameters, which are required for the main engine simulation to break the loops at the initial time step, are saved. These parameters can be better understood by dividing them in the following manner [53]:

(a) The known parameters;
(b) The (arbitrarily) set parameters;
(c) The unknown parameters.

The first category is simply known data such as the number and size of cylinders, type of engine, compression ratio, etc. This data is usually available from the engine manufacturers (found in the engine specifications guide). The second category of parameters is estimated, for instance, by expressing them non-dimensionally as a function of a known parameter. Examples are engine dimensions that are difficult to obtain (valve diameter, inlet and exhaust manifold diameters, etc.). These parameters can be set to a certain percentage of bore diameters. Their values can also be obtained from the engine test setup, if available.

The last category of parameters is mostly parameters that are intrinsic to the model and needed to simulate a certain phenomenon that is present in the real (full scale) system. For example, the 'mu-phi' parameter, a product of resistance/loss and contraction factor in the inlet and outlet valves; is used to determine the flow through the engine. The 'mu-phi' parameter is estimated to find the correct compressor size and thus, match the air-swallow characteristic of the compressor to that obtained from measurements. Furthermore, for an integrated system several subsystems need to perform optimally. For this purpose, some parameters (for instance, flow areas, piping lengths) need to be sized such that certain requirements are met. This is matching of the subsystems or briefly "system matching", which is a key activity in system integration. Such a matching also needs to be performed for the MVEM.

The analytical turbine and compressor models have some unknown parameters that need to be estimated to match the performance of the turbocharger and the diesel engine. This matching has been divided into the following three parts:

(i) Matching the compressor flow to the engine inlet flow at the appropriate inlet receiver pressure and compressor and engine speed. This means matching the air-swallow characteristic of the compressor.

(ii) Matching the turbine flow to the engine exhaust flow at the appropriate exhaust receiver pressure and temperature and turbine and engine speed. This means matching the turbine characteristic.

(iii) Matching the turbine power to the compressor power. This ultimately boils down to the Büchi balance which links the inlet receiver pressure to the outlet receiver pressure as built up by the turbine and given the inlet temperature before the turbine in relation to the compressor inlet temperature.

Using the above discussed parameters and method, the MVEM was calibrated and matched to simulate the performance of the test engine. A number of parameters were iteratively adjusted while comparing the simulation results with the test-bench measurements. In the remainder of this section, simulated engine parameters have been compared with test-bench measurements to showcase the calibrated and matched MVEM simulating the performance of the test-engine only for the case of no external back pressure. In the next section, the calibrated and matched model is validated against measurement with external back pressure.

The first proof of a good match between simulation and measurements is visible from Fig. 3.1(a) and (b). These figures present the compressor performance of the engine, obtaining the correct air flow for the corresponding pressure. For a good matching, it is also essential to simulate the temperatures as accurately as possible.

Fig. 3.2(a) compares the simulated and measured inlet receiver temperature. The maximum error between the simulated and measured inlet receiver temperature is about 5 percent at 100 percent load. Furthermore, Fig. 3.2(b) shows a good estimation of turbocharger speed.

The objective of a turbocharger model is to estimate the correct charge pressure and flow. However, it is also vital to estimate correct turbine pressures and temperatures. As explained earlier, the MVEM was applied to simulate the performance of a pulse turbocharged engine, which is not a mean value system and corrections had to be applied to the model. This gives deviations between simulated and measured turbine performance parameters. On the other hand, a constant pressure system (currently used turbocharger technology) would have a constant pressure in the outlet receiver, before the turbine, making it easier to simulate for a mean value model like the MVEM. Thus, the model would perform better with a constant pressure turbocharger system.
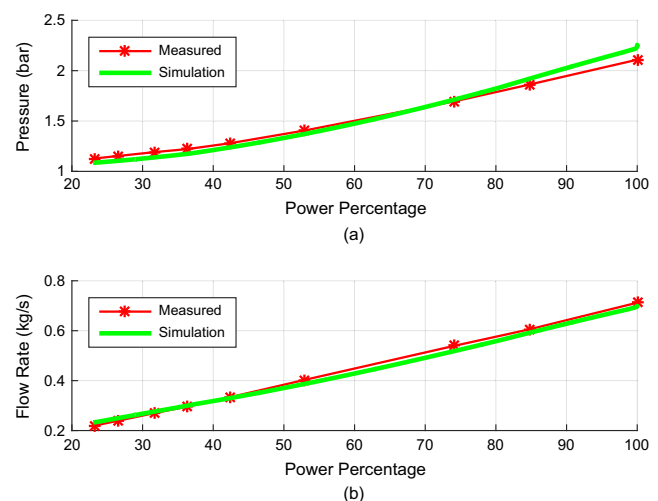

Fig. 3.1. Comparison between measured and simulated inlet receiver pressure (a), and air mass-flow rate (b).
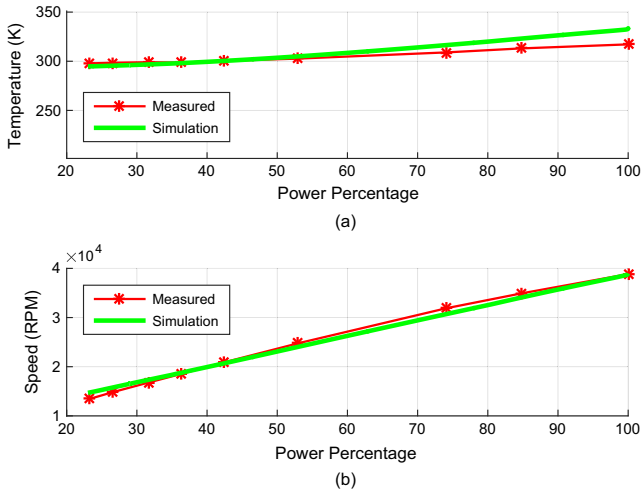
Fig. 3.2. Comparison between measured and simulated inlet receiver temperature (a), and turbocharger speed (b).

Fig. 3.4. Comparison between measured and simulated values of lowest turbine inlet pressure.
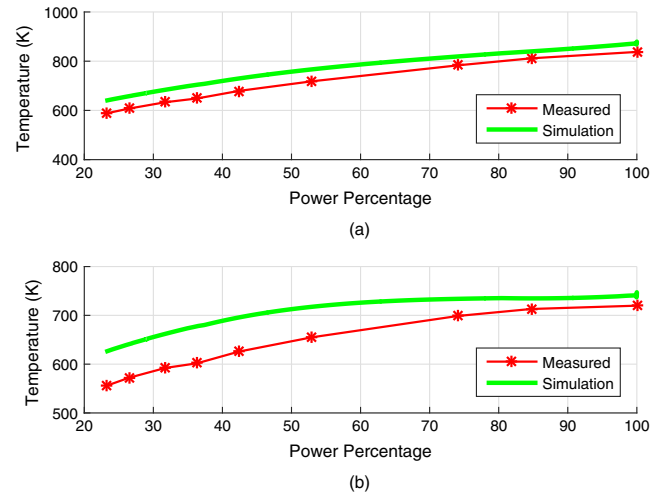
Fig. 3.5. Comparison between measured and simulated turbine inlet (a), and outlet temperatures (b).

Focussing back to the validation, Fig. 3.3 shows the comparison between the values of α and β, simulated (explained in 2.3) and the correction factors calculated for the measured turbine pulses, shown in Table 2.2.

As seen in Fig. 3.3, the β factor increases at part loads (or engine speeds along the propeller curve), implying an increase in work delivered by the turbine to the compressor. This is because at part loads the pulse factor increases, which increases the β value and decreases α. The increase in turbine work at part load is followed by an increase in the charge pressure and, hence, air flow rate, compared to the modern constant pressure systems. This difference in air flow rate delivered by a pulse and a constant pressure system can be very crucial against high back pressure and is discussed in detail in Section 5. At the same time, the flow through the turbine drops, as the α factor drops with decreasing load. This is in alignment with the working principle of a pulse turbocharging system, which is known to improve part load performance of diesel engines by increasing the incoming flow-rate of air [54].

However, as the MVEM is a mean value model, the turbine inlet pressure can closely simulate any one single value on the pressure pulse. Thus, an iterative method was adopted, where the turbine inlet pressure was matched to either the maximum or the mean
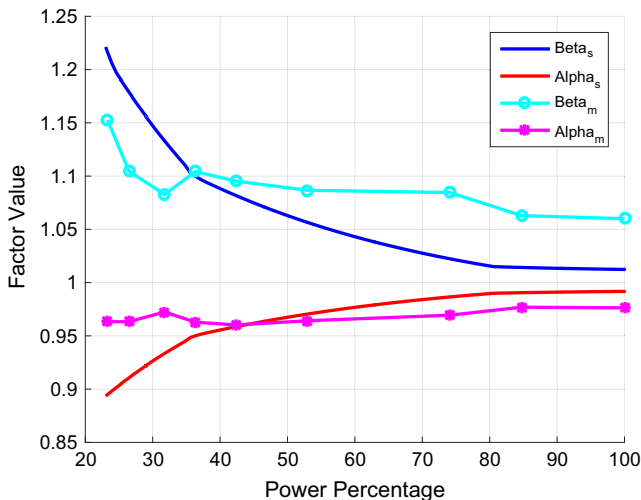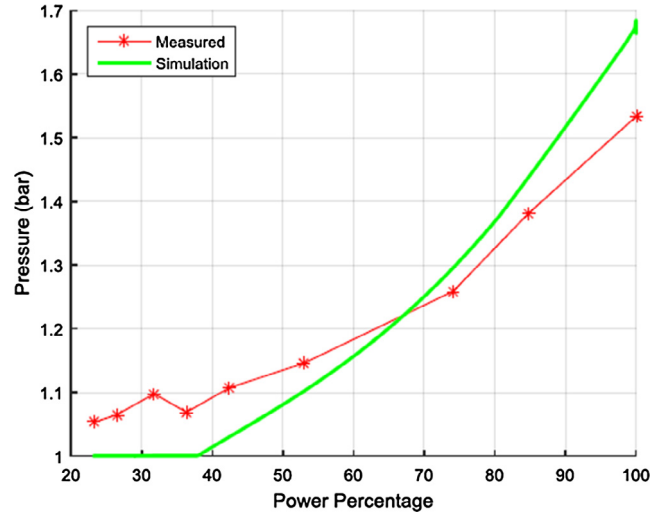
or the minimum pulse pressure, by changing a number of parameters in the turbocharger model. The criterion for this matching is to acquire the correct charge pressure and incoming air flow rate (Figs. 3.1–3.3) as well as turbine temperature estimations, within 15 percent deviation from the measurements. Following this method, it was found that the model gave best results, for the above criterion, when turbine inlet pressure was made to simulate the lowest pulse pressure. This can be seen in Figs. 3.4 and 3.5.

In Fig. 3.4, the turbine inlet pressure shows a maximum deviation of about 10 percent, while the increasing trend of the measurements is well depicted by the model simulation as well. Besides this, the turbine inlet temperature gives a maximum percentage difference of about 9 percent, at lowest load, and a difference of about 12 percent for turbine outlet temperature, as seen in Fig. 3.5(a) and (b).

This concludes the calibration and matching of the MVEM to simulate the performance of the pulse turbocharged test engine. This section also highlighted the shortcomings of the model related to the difficulty in simulating the pressure pulse. However, in a separate study this mode successfully simulated the performance of an engine running with a constant pressure turbocharger system [20].

Fig. 3.3. Comparison between α, β values obtained from simulation (s) and values calculated from measurements (m).

4. Validation of MVEM: effects of back pressure on engine performance

After calibrating and matching the MVEM to simulate the performance of the pulse turbocharged test engine with no external back pressure, the model was tested to predict the engine performance against back pressures of 0.25 mWC and 0.5 mWC. The model was further used to simulate the engine performance at rated set-point (360 kW at 1000 rpm), which could not be studied experimentally. This section focuses on the effects of back pressure based on these simulation tests and also measurements for the same values of externally applied back pressure.

Back pressure is the pressure measured at the turbine outlet. Thus, an increase in back pressure means an increase in turbine outlet pressure, marking the turbocharger (turbine) as the first defence line. An increase in turbine outlet pressure results in a decrease of turbine pressure ratio [13], as this is defined as pressure at turbine inlet over outlet. A drop in turbine pressure ratio reduces the power delivered by the turbine, and slows down the turbocharger. This decrease in turbocharger speed at higher back pressures is seen in Fig. 4.1, along with the turbo speed trend predicted by the model.

The measurements give a maximum decrease of about 4.4 percent, while the simulations calculated a decrease of about 5.5 percent for the same load point, at lowest load. Thus, the effect of steady-state back pressure on turbocharger speed is small.

The balance of power between compressor and turbine is used to calculate the charge pressure that can be delivered by the compressor. The charge pressure (obtained from compressor pressure ratio) is calculated as a function of turbine pressure ratio and other turbocharger variables, as shown in Eq. (11) [44].

$$\pi_{com} = \left\{ 1 + \beta \cdot \delta \cdot \chi \cdot \eta_{TC} \cdot \tau_{TC} \cdot \left(1 - \frac{1}{\pi_{tur}^{\frac{\gamma_{gas}-1}{\gamma_{gas}}}} \right) \right\}^{\frac{\gamma_{air}}{\gamma_{air}-1}} \quad (11)$$

where π_{com} = compressor pressure ratio, π_{tur} = turbine pressure ratio, β = pulse factor, $\delta = 1/(1 + afr)$, afr = air-fuel ratio, χ = ratio of specific heats of gas and air, η_{TC} = turbocharger efficiency, τ_{TC} = turbocharger temperature ratio, and γ = ratio of specific heats.

This equation is sometimes called as the "Büchi equation", and the β factor takes into account the effect of extra power delivered by the pulse turbocharger, which is also called the "Büchi turbocharger system" [55]. Eq. (11) shows that a decrease in
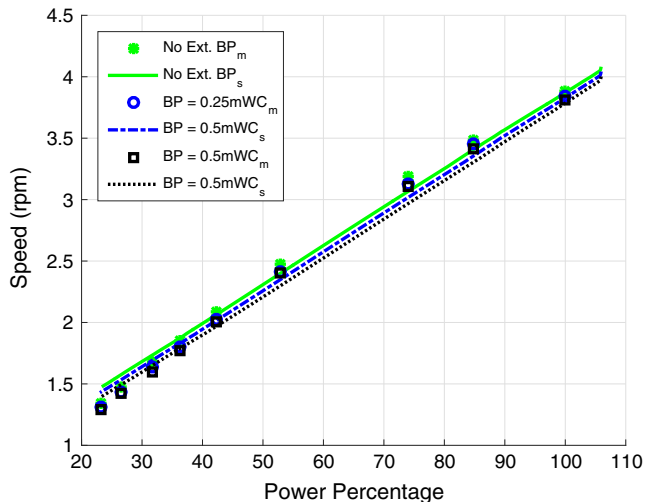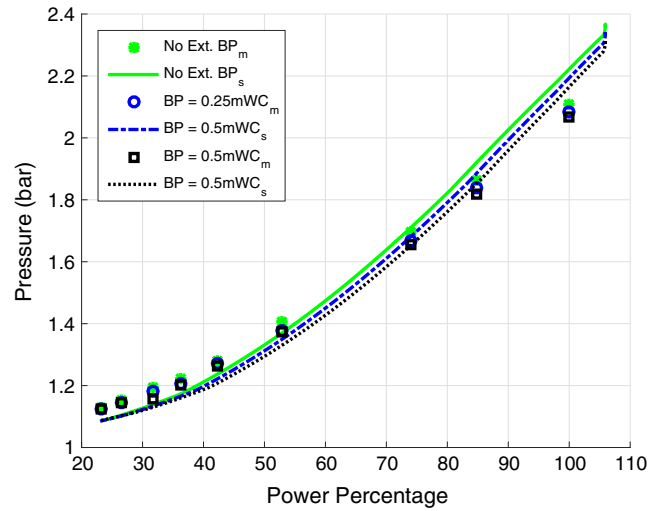

Fig. 4.2. Back pressure effect inlet receiver pressure based on measurements (m) and simulations (s).

turbine pressure ratio causes the compressor pressure ratio to reduce. A drop in compressor pressure ratio leads to a decrease in the inlet receiver pressure and also the air flow through the engine as shown in Figs. 4.2 and 4.3, respectively.

Once again, the simulations and measurements show a minor effect on the inlet receiver pressure and air flow rate. The trends of inlet receiver pressure and air-flow rate simulated by the MVEM deviate from test-bench measurements by a maximum of 6 percent. Even though the effects on the compressor side due to increasing back pressure are small, the effects are more noticeable and critical on the turbine side, especially the effect on turbine temperatures.

Increased back pressure means the engine would need to do more work to pump out the exhaust gases. However, the load demand from the water-brake remains constant. This decelerates the engine, activating the governor, which pushes in more fuel in order to offset the deceleration. Thus, an increase in back pressure would increase the fuel consumption. Simulations and measurements exhibited a small increase in fuel consumption of about 3 percent at 42 percent load and 0.5 mWC of back pressure. Fig. 4.4 shows the minor increase in fuel consumption due to increased back pressure.

Fig. 4.1. Back pressure effect on turbocharger speed based on measurements (m) and simulations (s).
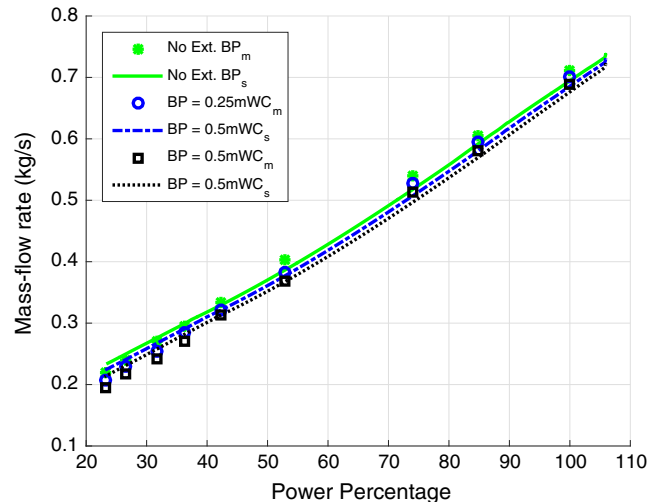

Fig. 4.3. Back pressure effect on air mass-flow rate based on measurements (m) and simulations (s).
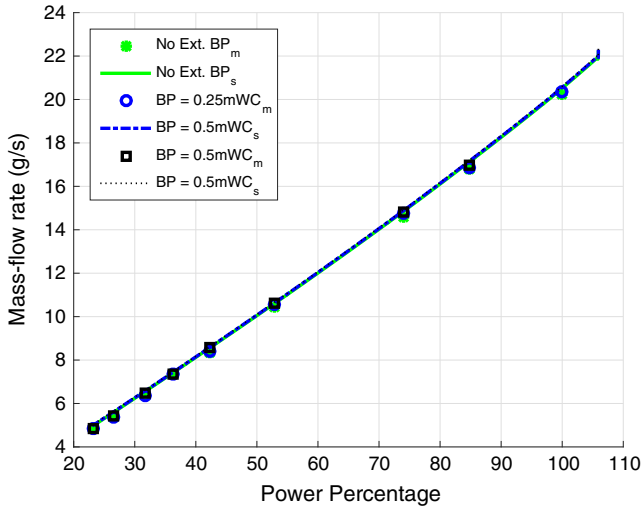
Fig. 4.4. Back pressure effect on fuel consumption based on measurements (m) and simulations (s).
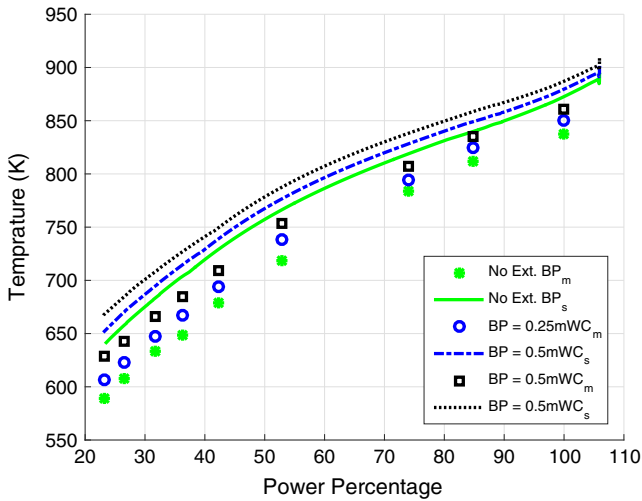

Fig. 4.5. Back pressure effect on turbine inlet temperature based on measurements (m) and simulations(s).

Therefore, back pressure causes an increase in fuel consumption (even though small) and drops air intake, leading to incomplete combustion and increase in in-cylinder and exhaust receiver temperatures, as seen in Fig. 4.5. Measurements and simulations show that the rise in turbine inlet (exhaust receiver) temperature due to back pressure is more significant at lower loads than at higher loads. Based on measurements, turbine inlet temperature increased by a maximum of 6.7 percent at lowest load; and by 4.5 percent based on simulations. Thus, the relative increase in temperatures predicted by simulations matched the measured. Excessive exhaust gad (exhaust receiver) temperatures can increase thermal stresses and cause serious damage to the turbocharger. Excessive exhaust temperatures can damage seals and grooves causing unintended oil and exhaust gas leakage [56]. High exhaust gas temperatures can also lead to a coked centre housing, which will affect turbocharger performance and life [57].

It is clear that the MVEM is satisfactorily able to predict performance of the test engine, with and without externally applied back pressure. Based on this validation, the MVEM was made to simulate the performance of the test engine with different turbocharger configurations and valve overlaps to tackle high values of back

pressure. The next section discusses the results of these simulations while describing a methodology to define acceptable limits of back pressure for any engine.

5. Discussion: defining back pressure limits

The previous section showed that back pressure causes a drop in incoming air, increases fuel consumption and raises outlet receiver temperatures. Out of these, the effect on fuel consumption was found to be small; however, increased outlet receiver temperatures and decreased air intake could have alarming effects on turbocharger performance (damage to oil seals, coked housing) and the environment (smoke). Another parameter that is strongly affected by back pressure is the exhaust valve temperature. The increase in exhaust valve temperature and exhaust receiver (turbine inlet) temperature can be used as an indicator of thermal overloading of the engine [58,59]. Furthermore, a diesel engine also needs a minimum amount of incoming air, i.e., low air-excess ratios can lead to high exhaust receiver temperatures (thermal overloading) and engine smoking [60,61]. These boundaries of smoke and thermal overload can be further used to find limits of back pressure that are acceptable for an engine, which will be covered in this section.

5.1. Smoke and thermal overload limit

Back pressure reduces the air intake of the engine. This air intake of a turbocharged, 4-stroke diesel engine can be divided into mainly two parts. Part one is the air that enters the cylinder during the induction process, the downward suction stroke of the piston. The second (smaller) part of the air-mass in the cylinder can be considered to come from the scavenging process, during the overlap of inlet and exhaust valves. The total fresh air mass ending up in the cylinder (m_{fresh}) is, therefore, a larger percentage of the induction mass flow and a smaller percentage of the trapped scavenging mass. The ratio of total fresh air mass in the cylinder to the minimum amount of air required for combustion ($m_{a,min}$) is defined as air-excess ratio (λ) [62], and

$$\lambda = \frac{m_{fresh}}{m_{a,min}} \qquad (12)$$

The air-excess ratio can be used as an indicator to define the smoke limit of an engine. In order to define such a limit, lines of constant air-excess ratio were drawn in a static engine map. In order to capture constant lines of engine performance parameters (air-excess ratio, charge pressure, exhaust valve temperature) in a static engine map; the model was run at different engine speeds and loads to cover the operating limits of the static engine map prescribed by the engine manufacturer. Fig. 5.1 shows the grid of simulated engine speeds and load settings (blue markers) along with approximate engine operating limits (black line) given by the engine manufacturer, representing the static map of the engine.

In this manner, the model was made to simulate the performance of an engine (same rating, size and 100 degree valve overlap) with a constant pressure turbocharger, which is more widely accepted than the old pulse turbocharger system. Fig. 5.2(a) shows the lines of constant air-excess ratio and Fig. 5.2(b) captures lines of constant charge pressure calculated within the operating envelope of the engine.

Fig. 5.2(a) shows that the lines of constant air-excess ratio within the engine map are more concave than a typical engine limit as given by the engine manufacturer, with a decreasing trend along constant engine rpm and increasing engine power. As mentioned earlier, an increase in back pressure reduces charge pressure
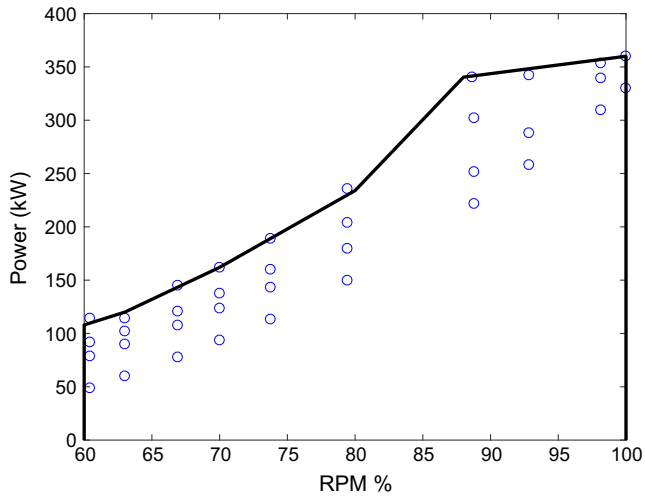
Fig. 5.1. Simulated load and engine rpm points (blue points) along with engine envelope (black line). (For interpretation of the references to colour in this figure legend, the reader is referred to the web version of this article.)

and decreases air-excess ratio. For higher values of back pressure, the air-excess ratio can lie far beyond the values associated with the smoke limit. Although it is not possible to measure air-excess ratio directly, it can be related back to charge pressure, which can also be plotted in the static engine map as shown in Fig. 5.2 (b). Nowadays, in most engines charge pressure is used as a measure of fresh air mass, and when divided by fuel rack it results in an approximate air-excess ratio.

In addition to using lines of constant air-excess ratio to define the smoke limit, the perhaps more important thermal overloading of the engine could be characterized by lines of constant exhaust valve temperature in a static engine map of power and engine speed. For this purpose, an exhaust valve temperature estimator ($T_{ev,est}$) was introduced into the MVEM, which is based on the formulation given in [58]. The total heating up of the exhaust valve is due to the heating during the blown down process and the successive cooling during the scavenging period of the engine. The temperature of the exhaust valve is estimated as a combination of cylinder temperature just before the opening of the exhaust valve (T_6), representing heating during blow down, and inlet receiver temperature (T_1), which represents cooling temperature during scavenging. Therefore, the exhaust valve temperature is estimated by the following equation:

$$T_{ev,est} = \frac{T_6 + r \cdot T_1}{1 + r} \tag{13}$$

$$r = s^{0.8} \cdot \left[\frac{T_1}{T_6}\right]^{0.25} \cdot \left[\frac{EC - IO}{IO - EO}\right]^{0.2} \tag{14}$$

where 'r' is a function of scavenge factor 's', blow down temperature (T_6), inlet receiver temperature (T_1) and ratio of the crank angle available for scavenging and for blow down. Scavenge factor 's' is defined as the ratio of the mean mass flow that goes through the engine during scavenging and the mean mass flow required for combustion.

The exhaust valve temperature estimator model introduced into the MVEM was used to simulate these temperatures for all the load and engine rpm points, shown in Fig. 5.1. Fig. 5.3(a) shows the lines of constant exhaust valve temperature. Like air excess ratio, the exhaust valve temperature cannot be easily measured in an actual engine. However, as a next best quantity the exhaust receiver temperature can be measured, and calculated contour curves are shown in Fig. 5.3(b).

As seen in these figures, the lines of constant exhaust valve and exhaust receiver temperature follow the characteristic of the limit curve, given by the engine manufacturer, much better than the contours of air-excess ratio presented in the previous figures. The hypothesis is that the exhaust valve temperature and, in its wake, the exhaust receiver temperature really capture thermal loading of an engine. Thus, giving a value of maximum allowable temperature defines a limit in the power/speed envelope and is a way to safeguard the engine from thermal overloading. It is evident from Fig. 5.2 that the lines of constant exhaust valve temperature and exhaust gas (exhaust receiver) temperature have the same trend, and hence both of them can be used to capture the effect of thermal overloading and define back pressure limits. In this paper, exhaust valve temperature has been adopted as an indicator for thermal overloading since it is considered to be the more critical quantity, however, exhaust receiver temperature can be measured in practice.

5.2. Application of smoke and thermal overload Limit: Defining acceptable back pressure

In order to better understand smoking and thermal overloading limits to define the ceiling for acceptable back pressure, the power on the y-axis and the quantities along contour lines in Figs. 5.2 and 5.3 were flipped, as presented in Fig. 5.4. These flipped graphs can be used to mark on their y-axis the values of maximum allowed
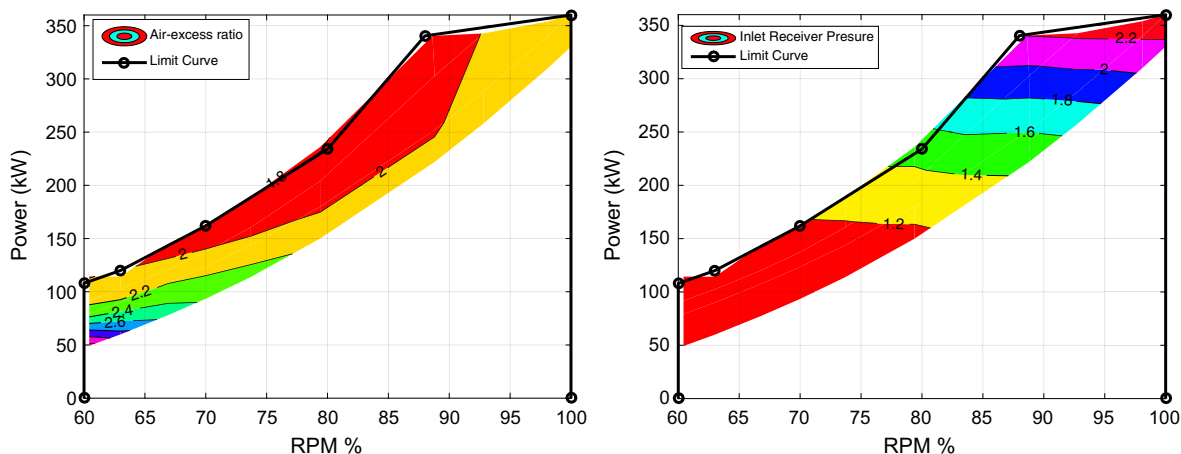

Fig. 5.2. Static engine map with lines of constant air-excess ratio (a), and lines of constant charge pressure (b) for a 100 degree valve overlap constant pressure turbocharged engine.
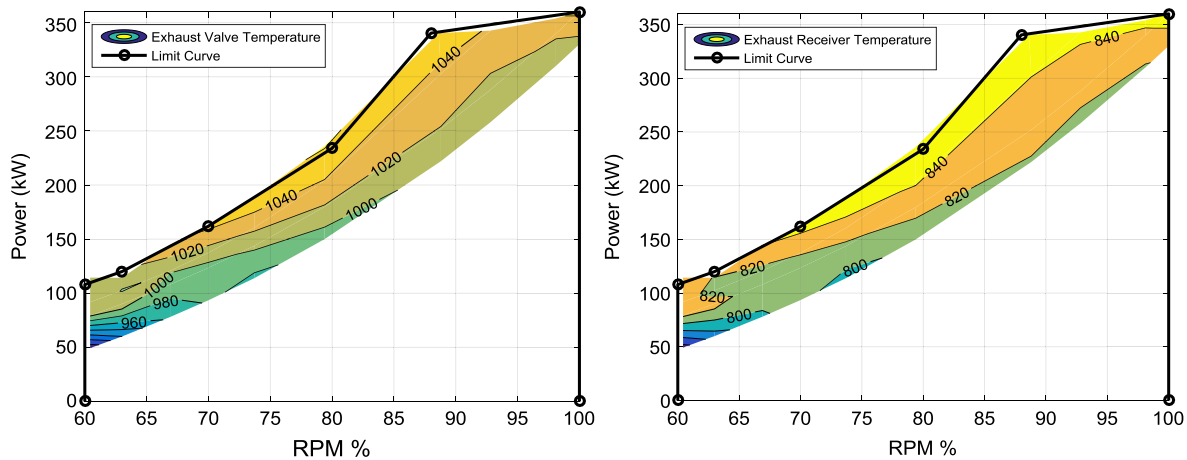
Fig. 5.3. Static engine map with lines of constant exhaust valve temperature (a) and constant exhaust receiver temperature (b) for a 100 degree valve overlap constant pressure turbocharged engine.
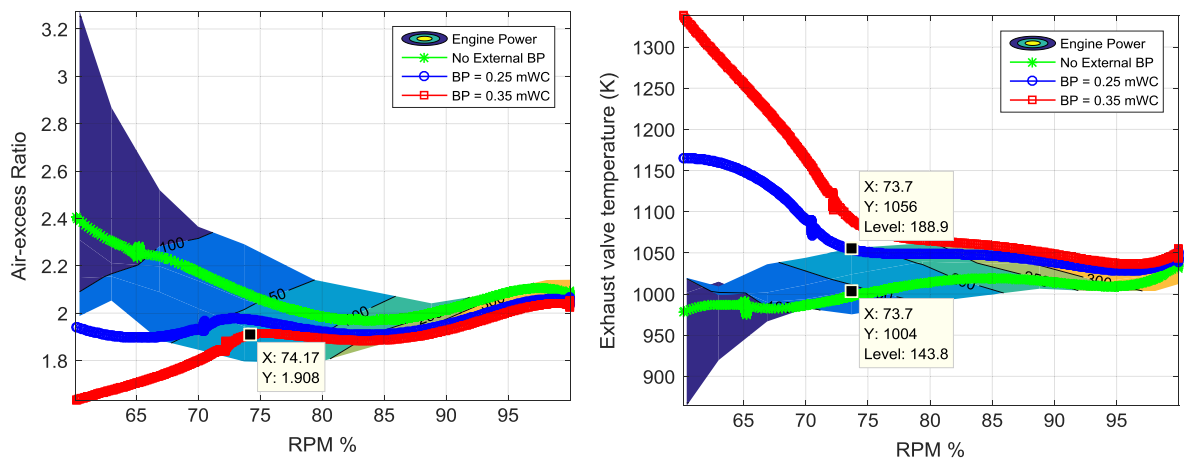

Fig. 5.4. Back pressure effect on air-excess ratio (a) and exhaust valve temperature of a constant pressure turbocharged engine, with 100 degree valve overlap.

air-excess ratio or exhaust valve temperature for each engine rpm and thus indicate the region where the engine could smoke or be thermally overloaded. The coloured area under the manufacturer's limit in Figs. 5.2 and 5.3 of course maps into a corresponding area in Fig. 5.4. Besides this, Fig. 5.4(a) and (b) also depict the decrease in air-excess ratio and increase in exhaust valve temperature due to increased external back pressure at constant power and speed. All the cases of increased back pressure have been simulated along the same propeller curve shown in Fig. 2.2.

Simulations show that for a back pressure of 0.35 mWC, the air-excess ratio could drop to alarmingly low values, and far into the region representing a relatively fuel rich mixture for a diesel engine, which could lead to engine smoking. Black engine smoke primarily contains elemental carbon (soot), which is considered to be the second-largest human contributor to climate change [63,64]. Additionally, black smoke can be a serious problem for a naval ship as it can increase the chances of detection. Fig. 5.4(a) illustrates that the air-excess ratio could drop drastically, thus indicating the possibility of engine smoke, especially at lower rpms [21]. The exhaust valve thermal overloading graph given in Fig. 5.4 (b) also shows that a back pressure of 0.35 mWC would be unacceptable for this engine and again the effect is most severe at low engine speed.

As seen in Fig. 5.4(b), the values of exhaust valve temperature for the case of no external back pressure lie within the limits of maximum allowable temperature at each engine rpm. However, the exhaust valve temperature, below 74 percent of engine speed, for back pressure of 0.25 mWC moves beyond the temperature limit obtained from the engine limit curve, thus, indicating thermal overloading and representing a back pressure limit. Besides defining limits of acceptable values of back pressure, the graph in Fig. 5.4(b) also provides two ways to avoid thermal overloading. One solution would be to reduce back pressure by switching from underwater to above water exhaust system at the point of thermal overload for a particular engine speed. For instance, for this engine it would be necessary to switch from underwater to above water exhaust at speeds below 75 percent. Furthermore, Fig. 5.4(b) shows that the effects of back pressure are more severe at lower values of engine speed, thus asserting a higher need to switch to above water exhaust systems at lower rpms than at higher rpms. Another solution would be to reduce the engine power at constant engine speed. For example, decreasing engine power along 74 percent engine speed can help reduce the temperature and avoid thermal overload. In this manner, the MVEM model can be used to define back pressure limits at any engine speed by applying the concept of smoke limit and thermal overloading.

The drop and knuckle seen at 74 percent engine speed (0.25 mWC) is because the pressure ratio across the engine at these points approaches 1. In other words, the pressure on the exhaust receiver side is almost equal to the pressure on the inlet receiver
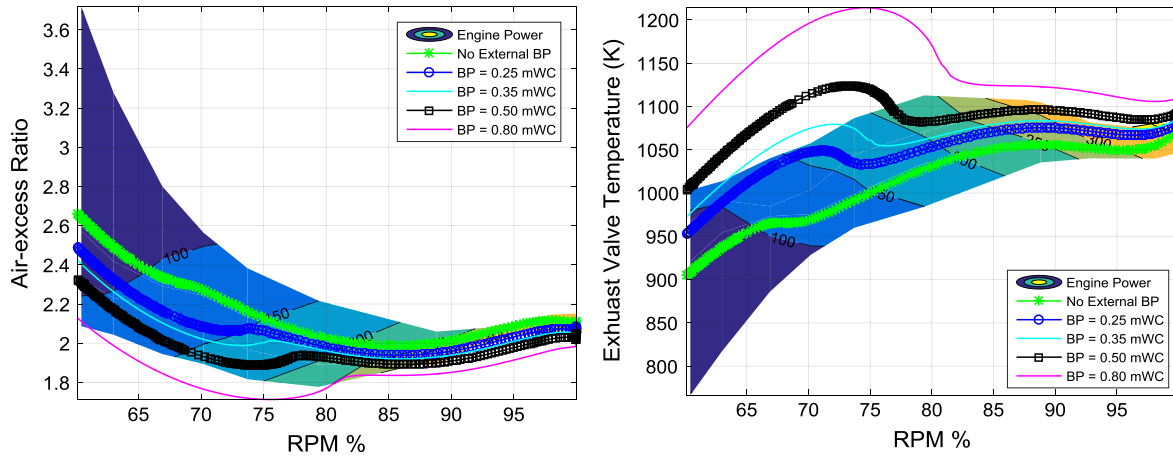
Fig. 5.5. Back pressure effect on air-excess ratio (a), and exhaust valve temperature (b) of a constant pressure turbocharged engine, with 30 degree valve overlap.

side. Flow direction of the engine fluctuates giving the knuckle. After this point, the engine experiences negative scavenging, and the flow reverses during the 100 degree valve overlap [27]. This causes a further loss of trapped fresh air-mass, as the air inside the cylinder gets replaced by exhaust gas during scavenging. These trapped exhaust gases raise the temperature of trapped mass at the beginning of compression, thus raising the overall in-cylinder and exhaust receiver temperatures. Additionally, negative scavenging creates a counter pressure at the compressor outlet, pushing the compressor towards compressor surge, which can damage the compressor [65].

An engine with a smaller valve overlap could reduce the negative scavenging and keep the air-excess ratio from dropping too low. Fig. 5.5(a) shows the improvement in the air-excess ratio characteristic, predicted by the MVEM for the same engine with a 30 degree valve overlap and constant pressure turbocharger system. This proves that an engine with a smaller valve overlap will be able to handle higher values of back pressure. A 30 degree valve overlap increases the amount of total trapped air in the cylinder in two ways. First, it increases the amount of induction air as the exhaust valve closes earlier than in the case of 100 degree valve overlap (assuming that the inlet valve opens at the same moment for both the cases). Secondly, a small overlap means reduced negative scavenging and more trapped air compared to a larger valve overlap. However, the higher the back pressure, the lower the charge pressure, meaning the point of negative scavenging is reached at a much higher power percentage. This reduces the

excess air and gives the peculiar characteristic of the lambda curve, shown in Fig. 5.5(a). The improved air-excess ratio due to reduced valve overlap helps reduce exhaust valve temperatures and this is clearly evident in Fig. 5.5(b). As seen in Fig. 5.5(b), the engine can now easily handle higher back pressure of 0.25 mWC without any thermal overloading and also 0.35 mWC of back pressure at most engine speeds. The effect of back pressure is, once again, more pronounced at low engine rpms, and the speed where back flow is initiated creeps up. The need to switch to above water exhaust is evident at low engine speeds.

In order to improve the back pressure handling capabilities at low rpms, it is important to further increase the air-intake of the engine, which would require higher charge pressures. As explained in Section 2 and Section 3, the pulse turbocharger system delivers extra work to the compressor. The extra work or β factor helps keep the charge pressure high (Eq. (11)), and also the amount of total air in the cylinder. In pulse turbocharger systems, this extra work is most effective at part loads (or engine speeds along the propeller curve), as shown in Fig. 3.3, and hence keeps the air-excess ratio from dropping at these loads. On the other hand, in a constant pressure system, the pressure pulses are collected in an exhaust receiver before entering the turbine, the turbine inlet pressure drops to a lower and a constant value in contrast to that of a pulse system. Since, the pressure at the turbine inlet is constant, in case of constant pressure turbochargers, there is an absence of extra work delivered due to the pulse, making the β equal to 1 [44]. Fig. 5.6 shows the simulated increase in inlet recei-
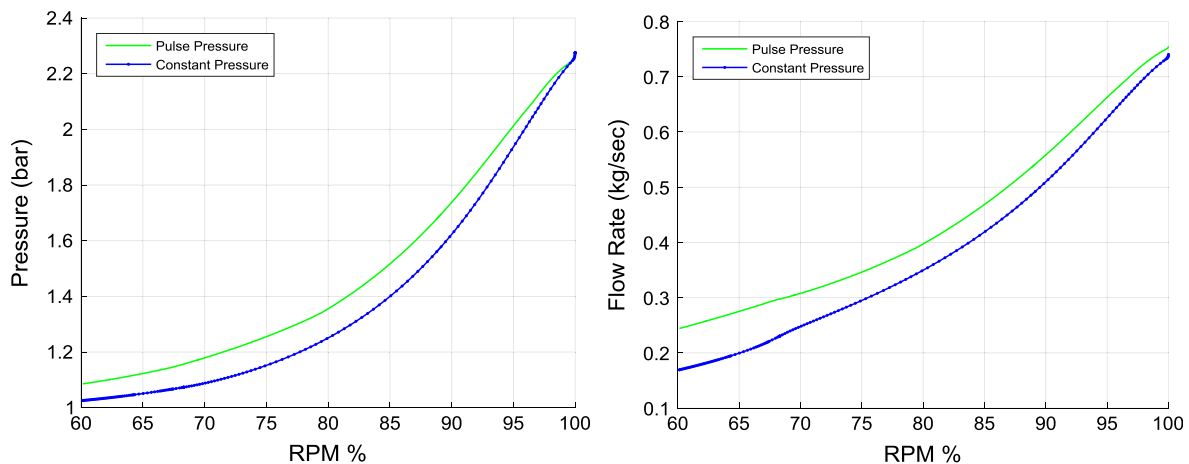

Fig. 5.6. Comparison between inlet receiver pressure (a) and air mass-flow rate (b) delivered by a pulse turbocharger and constant pressure turbocharger, with a 30 degree valve overlap engine.
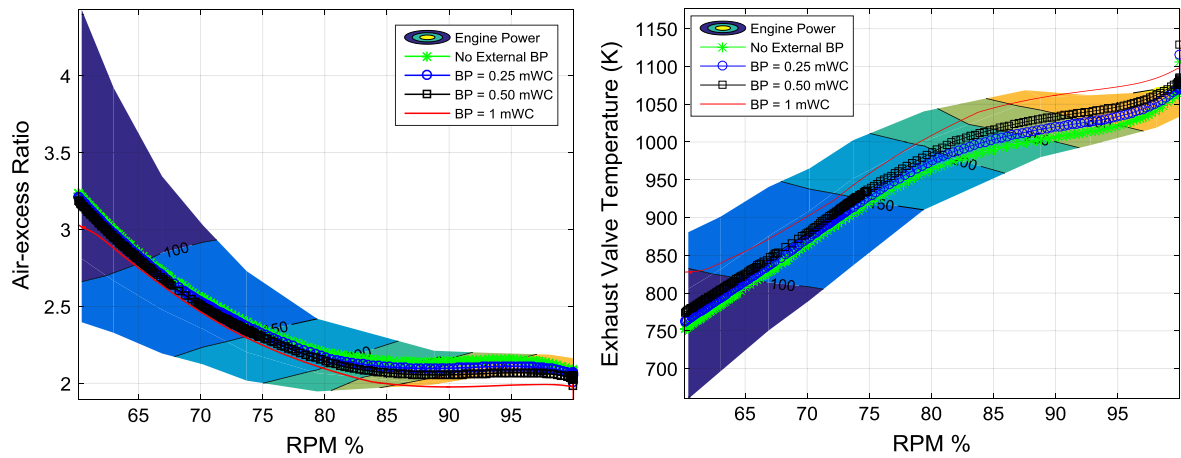
Fig. 5.7. Back pressure effect on air-excess ratio (a) and exhaust valve temperature (b) of a constant pressure turbocharged engine, with 30 degree valve overlap.

ver pressure and air mass-flow rate for a 30 degree valve overlap engine with a pulse turbocharger compared to the constant pressure turbocharger engine, when no external back pressure is applied.

Fig. 5.6 shows that at rated speed the pulse turbocharger and constant pressure turbocharger have almost equal values of inlet receiver pressure and air flow rate. However, at lower rpms (or load along the propeller curve) the pulse system delivers much higher values of charger pressure and air intake compared to the constant pressure turbocharger. Simulations show that the air intake for a pulse turbocharger is more by 68 percent, at lowest speed, when compared to that delivered by a constant pressure system. This drastically improves the back pressure handling capabilities of the engine as depicted in Fig. 5.7.

As evident in Fig. 5.7, the 30 degree valve overlap engine with a pulse turbocharger can sustain 1 mWC of back pressure with signs of thermal overloading only above 90 percent engine speed. Furthermore, Fig. 5.7 shows that the air-excess ratio of a pulse turbocharged engine hardly drops below 1.9 at a back pressure of 1 mWC, indicating no signs of engine smoke. The model shows that such a system would easily be able to counter the high values of back pressure due to the pulse effect, and also reduced back flow in case of any negative scavenging (smaller valve overlap). This would cancel the need to switch to an above water exhaust, at lower rpms.

This section shows that both smoke and thermal overloading, simulated by the MVEM, can be used as an indicator to define limits of acceptable back pressure at any engine speed. A thermally overloaded engine can be unloaded by either reducing engine power or back pressure. This section also proves that a pulse turbocharged engine and a small overlap can drastically help improve back pressure handling capabilities of an engine compared to a constant pressure turbocharger system and large valve overlap.

6. Conclusions

This paper provides a detailed understanding of back pressure effects on engine performance, when running against high back pressure (especially, for underwater exhaust systems). The effects were analysed based on test-bench measurements performed on a pulse turbocharged diesel engine and model simulations. The conclusions drawn from this study are as follows:

- The study found that air-excess ratio, exhaust receiver and exhaust valve temperature are the most critical engine parameters against high back pressure. The effect on fuel consumption was found to be less significant.

- Back pressure effects on air-excess ratio, exhaust receiver and valve temperatures were more pronounced at lower engine speeds (or loads along the propeller curve). Effects were inconsequential at high engine speeds, suggesting that engine performance at lower speeds needs more attention than that at higher speeds, when exhausting underwater.

- Exhaust valve temperature and exhaust receiver temperature could be used to quantify thermal overloading of the exhaust valve and tubine blading, respectively. A method was presented that can be applied in practice by using a conceptual model of the smoke limit as well as thermal overloading to define acceptable limits of back pressure for an engine.

- Simulation results showed that an engine with a large valve overlap, and a constant pressure turbocharger, exhibits a drastically decreased air-excess ratio at low speeds even at relatively low levels of back pressure. Additionally, the engine was also found to be thermally overloaded again, at low speeds and same values of low back pressure.

- An engine with a constant pressure turbocharging system and a small valve overlap is able to sustain higher back pressures compared to an engine with a large valve overlap. Thermal overloading was found at low speeds, thus showing a need to temporarily switch to an exhaust above the water, when using an underwater exhaust systems and constant pressure turbochargers.

- Interestingly, the study also found that a pulse turbocharged engine with a small valve overlap is better at handling high back pressure than the modern, constant pressure turbocharged engines with the same valve overlap.

This research also shows that a relatively simple Mean Value Engine Model can provide vital engine performance information to yacht builders, shipyards, engine manufacturers and the exhaust system manufacturers, to optimize engine and ship performance.

Acknowledgements

References

[1] Heywood JB. Internal combustion engine fundamentals. New York: McGraw-Hill; 1988.
[2] Ra Y, Reitz RD. A combustion model for IC engine combustion simulations with multi-component fuels. Combust Flame 2011;158(1):69–90.
[3] López SG. Three-zone in-cylinder process model for DI diesel engines. Delft University of Technology; 2014.
[4] Raptotasios SI, Sakellaridis NF, Papagiannakis RG, Hountalas DT. Application of a multi-zone combustion model to investigate the NOx reduction potential of two-stroke marine diesel engines using EGR. Appl Energy 2015;157:814–23.
[5] Theotokatos G, Tzelepis V. A computational study on the performance and emission parameters mapping of a ship propulsion system. Proc Instit Mech Eng Part M J Eng Marit Environ 2015;229(1):58–76.
[6] Jensen J-P, Kristensen AF, Sorenson SC, Houbak N, Hendricks E. Mean value modeling of a small turbocharged diesel engine. In: SAE Technical Paper; 1991.
[7] Scappin F, Stefansson SH, Haglind F, Andreasen A, Larsen U. Validation of a zero-dimensional model for prediction of NOx and engine performance for electronically controlled marine two-stroke diesel engines. Appl Therm Eng 2012;37:344–52.
[8] IMO. MARPOL ANNEX VI and NTC 2008 with guidelines for implementation – supplement, vol. 258, no. September 2015; 2015. p. 1–24.
[9] MarQuip BV. Emission Technology. [Online]. Available: http://www.marquip.nl/exhaust-systems-expertise/emission-technology [accessed 06.03.17].
[10] Vejlgaard-laursen M, Olesen HR. (Diesel & Turbo, "Controlling Tier III Technologies. In: 28th CIMAC World Congress; 2016, p. 9.
[11] Wärtsilä. Wärtsilä Environmental Product Guide. Finland; 2015.
[12] Tauzia X, Chessé P, Maiboom A. Simulation study of a ship's engine behaviour running with a periodically immersed exhaust. Proc Inst Mech Eng Part M J Eng Marit Environ 2008;222(4):195–205.
[13] Hield P. The effect of back pressure on the operation of a diesel engine; 2011.
[14] "Ricardo Software - WAVE - Engine performance." [Online]. Available: https://www.software.ricardo.com/Products/WAVE/WAVE-engine-performance [accessed 06.03.17].
[15] Swain E. Turbocharging the submarine diesel engine. Mechatronics 1994;4(4):349–67.
[16] Michos CN, Lion S, Vlaskos I, Taccani R. Analysis of the backpressure effect of an Organic Rankine Cycle (ORC) evaporator on the exhaust line of a turbocharged heavy duty diesel power generator for marine applications. Energy Convers Manage 2017;132:347–60.
[17] Joardder MUH, Uddin MS, Roy MM. Effect of engine backpressure on the performance and emissions of a CI engine.
[18] Cong S, Garner CP, Mctaggart-Cowan GP. The effects of exhaust back pressure on conventional and low-temperature diesel combustion. Proc Instit Mech Eng Part D J Automob Eng 2011;225(2):222.
[19] Mittal M, Donahue R, Winnie P. Evaluating the influence of exhaust back pressure on performance and exhaust emissions characteristics of a multicylinder, turbocharged, and aftercooled diesel engine. J Energy Resour Technol 2015; 137(3): 032207.
[20] Sapra HD. Study of effects on diesel engine performance due to varying back pressure for an underwater exhaust system. Delft University of Technology; 2015.
[21] Burnete N, Moldovanu D, Baldean D-L, Kocsis L. Studies regarding the influence of exhaust backpressure on the performances of a compression ignited engine. Proc Eur Autom Congr EAEC-ESFA 2015;2015:141–9.
[22] Woods W, Woods D. Submerged exhaust discharge for marine vessel. US20100041288 A1; 2010.
[23] Bertin & Cie. Underwater exhaust device for the internal combustion engine of a vessel. WO19930070053 A1; 1993.
[24] Nelson H, Mullins W. Under-water exhaust for launches. US900576A; 1908.
[25] Bolt J, Bergin S, Vesper F. The influence of the exhaust back pressure of a piston engine on air consumption, performance, and emissions. SAE technical paper 730195; 1973.
[26] Adams TG. Effect of exhaust system design on engine performance; 1980.
[27] M.A.N, "M.A.N B&W: Operating Manual for Diesel Engines."
[28] Geertsma RD, Negenborn RR, Visser K, Hopman JJ. Pitch control for ships with mechanical and hybrid propulsion: modelling, validation and performance quantification. To be Publ.; 2017.
[29] Theotokatos G. A comparative study on the cycle mean value modelling of a large two-stroke marine diesel engine. Proc Instit Mech Eng Part M J Eng Marit Environ 2010;224(3):193–205.
[30] Hendricks E. Engine Modelling for Control Applications: A Critical Survey. Meccanica 1997;32(5):387–96.
[31] Guan C, Theotokatos G, Zhou P, Chen H. Computational investigation of a large containership propulsion engine operation at slow steaming conditions. Appl Energy 2014;130:370–83.
[32] Baldi F, Theotokatos G, Andersson K. Development of a combined mean value-zero dimensional model and application for a large marine four-stroke Diesel engine simulation. Appl Energy 2015;154:402–15.
[33] Tang Y, Zhang J, Gan H, Jia B, Xia Y. Development of a real-time two-stroke marine diesel engine model with in-cylinder pressure prediction capability. Appl Energy 2017;194:55–70.
[34] Benvenuto G, Campora U. Dynamic simulation of a high- performance sequentially turbocharged marine diesel engine. J Eng Marit Environ 2011;3(3):115–25.
[35] Pasini G et al. Evaluation of an electric turbo compound system for SI engines: A numerical approach. Appl Energy 2016;162(January):527–40.
[36] Gnana Sagaya Raj AR, Mallikarjuna JM, Ganesan V. Energy efficient piston configuration for effective air motion - A CFD study. Appl Energy 2013;102:347–54.
[37] Stratsianis V, Kontoulis P, Kaiktsis L. Effects of fuel post-injection on the performance and pollutant emissions of a large marine engine. J Energy Eng 2016;142(2):E4016001.
[38] Lalasangi S. Simulation of in-cylinder cold flow process of a piston bowl in a Di diesel engine using CFD. 2016; 9(3): 387–90.
[39] Shi W, Grimmelius HT, Stapersma D. Analysis of ship propulsion system behaviour and the impact on fuel consumption. Int Shipbuild Prog 2010;57(1–2):35–64.
[40] Miedema S, Lu Z. The dynamic behavior of a diesel engine. Proc. WEDA XXII Tech. Conf. 34th Texas A&M Dredg. Semin., no. June 2002; 2002.
[41] Schulten PJM (Royal Netherlands Naval College) and Stapersma D (Royal Netherlands Naval College & Delft University of Technology). Mean Value Modelling of the Gas Exchange of a 4-stroke Diesel Engine for use in powertrain applications; 2002.
[42] Schulten PJM, Toxopeus S, Stapersma D. Propeller - diesel engine interaction in a turn.
[43] Chen P, Flynn S. Development of a single cylinder compression ignition research engine. SAE Tech. Pap.; 1965.
[44] Stapersma D. Diesel engines : a fundamental approach to performance analysis, turbocharging, combustion, emissions and heat transfer including thermodynamical principles. Pt. 1. Diesel engines A : performance analysis and turbocharging: WB4408A. Vol. 2, Turbocharging," vol. 2; 2010.
[45] Schulten PJM (Royal Netherlands Naval College). The interaction between diesel engines, ship and propellers during manoeuvring; 2005.
[46] Ding Y. Characterising combustion in diesel engines. Delft University of Technology; 2011.
[47] Grimmelius HT, Mesbahi E, Schulten PJM, Stapersma D. The use of Diesel engine simulation models in ship propulsion plant design and operation. In: CIMAC; 2007.
[48] Dijkstra C. Description of Simulink mean value diesel engine model 'DEII', DMS 04/10, Internal report.
[49] Baan. Doorontwikkeling modulair simulatiemodel van een dieselmotor (IN DUTCH); 1998.
[50] Zinner D, Karl A. Aufladung von Verbrennungsmotoren, 2nd ed. Berlin, Heidelberg, NewYork: Springer-Verlag; 1980.
[51] Ligtvoet MPJ. The matching and validation of a mean value 4-stroke diesel engine model. TUD DMS04/06; 2004.
[52] Martijn Kom. Effect of pressure pulse in the exhaust receiver, PFS-196B, Internal report; 2006.
[53] Stapersma D. Calibrating and matching the mean value first principle diesel engine model (KIM-PFS-2011-188, Issue A and Issue B); 2015.
[54] Codan E, Vlaskos I, Kyrtatos N, Alexandrakis N. ABB Turbocharging Controlled pulse turbocharging of medium speed 5-cylinder diesel engines 2 Controlled pulse turbocharging of medium speed 5-cylinder diesel engines; 2005.
[55] Büchi AJ. Exhaust turbocharging of internal combustion engines: its origin, evolution, present state of development, and future potentialities. Lancaster, Pa., under the auspices of JOURNAL of THE FRANKLIN INSTITUTE.
[56] Idzior M, Karpiuk W, Bieliński M. Operating problems of turbocharging systems in compression-ignition engines. J. POLISH CIMAC.
[57] "KNOWING YOUR TURBOCHARGED DIESEL ENGINE." [Online]. Available: http://www.truckpro.com/Content/Resources/know-your-turbo.pdf [accessed 06.03.17].
[58] Grimmelius HT, Stapersma D. Control optimisation and load prediction for marine diesel engines using a mean value simulation model. ENSUS 2000, Conf. Proc.; 2000.
[59] Grimmelius HT, Stapersma D. The impact of propulsion plant control on Diesel engine thermal loading. Int. Counc. Combust. Engines Congr.; 2001. p. 89–100.
[60] Nanda S, Jia B, Smallbone A, Roskilly A. Fundamental analysis of thermal overload in diesel engines: hypothesis and validation. Energies 2017;10(3):329.
[61] Nanda SK, Jia B, Smallbone A, Roskilly AP. Investigation on the effect of the gas exchange process on the diesel engine thermal overload with experimental results. Energies 2017;10(6):766.
[62] Stapersma D. Diesel engines : a fundamental approach to performance analysis, turbocharging, combustion, emissions and heat transfer : including thermodynamical principles. Pt. 2. Diesel engines B : combustion, emissions and heat transfer : WB4408B. Vol. 3, Combustion. Delft: TU Delft; 2010.
[63] Juliet Eilperin et al. Black carbon ranks as second-biggest human cause of global warming; 2013.
[64] Bond TC et al. Bounding the role of black carbon in the climate system: A scientific assessment. J Geophys Res Atmos Jun. 2013;118(11):5380–552.
[65] Ali Ghanbariannaeeni and Ghazalehsadat Ghazanfarihashemi. Protecting a centrifugal compressor from surge. Gas Pipeline J 2012; 239(3).